Hetero-contact microstructure to program discerning tactile interactions for virtual reality

Xinqin Liao[a,1,*], Weitao Song[a,1], Xiangyu Zhang[a,1], Hongbing Zhan[b], Yue Liu[c,d], Yongtian Wang[c,d], Yuanjin Zheng[a,*]

[a] School of Electrical and Electronic Engineering, Nanyang Technological University, 50 Nanyang Avenue, Singapore 639798, Singapore.
[b] College of Materials Science and Engineering, Fuzhou University, 2 Xueyuan Road, Fuzhou 350108, China.
[c] Beijing Engineering Research Centre of Mixed Reality and Advanced Display, School of Optics and Photonics, Beijing Institute of Technology, 5 Zhongguancun South Street, Beijing 100081, China.
[d] AICFVE of Beijing Film Academy, 4 Xitucheng Road, Beijing 100088, China.

*Corresponding author
E-mail address: liaoxinqin677@163.com (X. Liao), yjzheng@ntu.edu.sg (Y. Zheng).
[1]These authors contributed equally to this work.

Abstract

Helping to reconstruct and restore tactile perception motivates the continuous development of functional materials, sensing structures, and manufacturing strategies. Coding and use of mechanotransduction signals from artificial tactile perception make a vital contribution to provide tactile feedback for robots, prosthetics, and rehabilitation therapy. Here we propose a hetero-contact microstructure (HeCM) to fabricate tactile sensor by using silver nanowires@polyurethane scaffold combined with layered carbon fabric. The synergistically perceiving of the HeCM enables the mechanosensational range of tactile sensor to be programmatically and significantly enhanced by >100% compared to the one of the common counterpart. The as-designed sensor characterizes high sensitivity, fast response time, and reproducible electromechanical properties to identify static and dynamic external pressure changes. Actual fingertip events can be converted into visual or audio interactive feedback in virtual reality by the intelligent sensor, demonstrating the feasibility and practicality of design concept and great potential of the sensor for human-interactive system.

Keywords: wearable devices, hetero-contact microstructures, tactile sensors,

human-machine interactions, virtual reality

1. Introduction

Somatosensation relies on cutaneous afferents to perceive surroundings and thus is crucial to perform many of our daily tasks involving emotional communication and execution of targeted action [1]. As one of the primary kind of somatosensation, tactile perception spreads over the entire body and shapes our interactions in object manipulation tasks [2, 3]. Imitating the sensory ability of living organisms to convert mechanical stimulus into an available signal creates the needed information about the physical properties of targeted objects [4, 5]. Ceaselessly pursued by material scientists, electromechanical scientists, neuroscientists, and medical scientists, coding and use of the mechanotransduction signals from artificial tactile perception make a vital contribution to provide tactile feedback for robots, prosthetics, and rehabilitation therapy [6-15]. Helping to reconstruct and restore tactile perception motivates the continuous development of functional materials, sensing structures, and manufacturing strategies [16-27]. Functional materials including micro/nanoparticles, one- or two-dimensional materials, and their composites with the capabilities that provide the electromechanical signal conversion of exteroceptive stimulus play a considerable role in the reconstruction and restoration of tactile perception, and thus enable the dexterous manipulation of objects and the discerning interaction of apparatus [28-31]. Efforts of sensing devices are mainly based on homo-contact microstructure (HoCM) that utilizes the microstructural contact between the same materials or within a single material as the sensing contact for the scientific and engineering researches of artificial tactile perception. However, the sensing mechanism of hetero-contact microstructure (HeCM) that bases on the microstructural contact between different types of materials is seldom reported where the influence on device's sensitivity and sensing range has yet to be studied.

Recent encouraging advances in manufacturing and design of HoCM enabled composite materials to realize tactile sensing functionality [32-42]. Synthesized from polymers swollen with an abundance of conductive ionic liquid, hydrogels could be

used to develop highly stretchable and transparent touch sensors for locating a finger on a deformable panel [32, 33]. Optionally, hollow-sphere microstructure, capsule-like framework, honeycomb-like foam, and porous sheet were proposed to construct pressure sensors that utilized conductive materials including graphene, carbon nanotubes, polypyrrole, and carbonaceous nanofibers [34-37]. Despite the significant progress, most of these sensors showed relatively narrow sensing range, which may restrict them in a wider range of future applications. Additionally, further identifying, coding and use of the mechanotransduction signals should be exploited and demonstrated.

Here we propose the HeCM to fabricate tactile sensors inspired by the synergistically sensory mechanism of mammalian tactile mechanoreceptors. The synergistically perceiving of HeCM enables the mechanosensational range of the tactile sensor to be significantly enhanced by >100% compared to the one of the counterpart based on the HoCM. The as-designed HeCM tactile sensor characterizes fast, stable, and reproducible electromechanical properties to identify static and dynamic external pressure changes. Wearable three-dimensional (3D) tactile panel with auxiliary analog-to-digital conversion circuit demonstrates the fascinating application of the HeCM tactile sensor in the field of human-machine interactions. Noteworthily, the coding and use of the mechanotransduction signal from the HeCM tactile sensor do not need any denoise processing or signal amplification that significantly reduces the difficulty of circuit design specially for multiple units integrated system and makes the competitive advantage compared to other sensors. As a proof-of-concept, the HeCM tactile sensor is served as the functional sensing medium of a data glove to turn actual fingertip events into specified interactions of virtual reality system, where precise and free control of virtual navigation is realized.

2. Experimental section

2.1. Materials and devices fabrication

PU scaffold (60 DPI, Hangzhou Meimei Electronic Commerce Co., Ltd.) was washed separately with ethyl alcohol and deionized water. After dried by air blowing,

the pure PU scaffold was cut as a rectangle (thickness of ~2 mm), and then put into the AgNWs solution (NJ-CW2001, Zhuhai Nanometals Technology Co., Ltd.). A hot plate with the set temperature of 30 °C was utilized to dry the wet PU scaffold that adsorbed the AgNWs solution due to capillary effect for half an hour. In order to turn the composite of AgNWs@PU scaffold to being active to achieve the pressure-sensitive characteristic, the loading force of >10 N was applied on it lasting for about 5 s. The resistance of the active composite of AgNWs@PU scaffold was influenced by the times of the soak-coating and drying process (Fig. S1). In this work, four times of the soak-coating and drying processes were chosen to fabricate tactile sensor. To fabricating the HeCM tactile sensor, two pieces of carbon fabric (WOS1009, CeTech Co., Ltd.) were respectively placed on the top and bottom of the active composite of AgNWs@PU scaffold for sandwiching assembly. The conductive wires were led out respectively on the top and bottom of the assembled materials by using conductive silver paint (SPI, YFS-05002). Finally, an adhesive tape (ScotchTM Magic Tape 810#, 3M Inc.) was used for encapsulation of the device. It should be noted that the device needed to be pinched in the horizontal direction to make the assembled materials in a weak contact. For comparison, the LM tactile sensor was made of two pieces of the carbon fabric, which were face-to-face assembled together. In the other case, the active composite of AgNWs@PU scaffold was directly employed to fabricate the PM tactile sensor. Both these tactile sensors used the same encapsulation method as the one of the HeCM tactile sensor.

2.2. Properties measurements and characterization

The material morphology was obtained by field-emission scanning electron microscopy (JEOL, JSM 6340F). The electrical signals of the sensors were read out by the standard digital multimeter (UNIT UT39B) and high precision digital multimeter (Agilent 34461A). Tests of the sensors under different dynamically cyclic pressure were performed by a designed actuator (Beijing Times Brilliant Electric Appliance Technology Co., Ltd.). The pressure was calibrated by the standard force sensor (Bengbu Sensors System Engineering Co., Ltd., JHBM-7). A

microprogrammed control unit (MCU, Arduino MEGA 2560) was employed to identify the electrical signal of the sensors and then make a conversion between digital signals and analog signals. A hot plate (WIGGENS, WH220 PLUS) was used to dry the composite of AgNWs@PU scaffold.

3. Results and discussion

The main fabrication steps of the HeCM tactile sensor are schematically illustrated in **Fig. 1**a. In this work, the PU scaffold was selected as the porous supporter due to its good softness and elasticity. As the selected PU scaffold was the form of interlaced bones and featured the small hole size of <600 μm (Fig. S2), AgNWs solution would be absorbed inside the PU scaffold due to capillary effect. The formation of the composite of AgNWs@PU scaffold included two main steps. First, the PU scaffold was immersed into the AgNWs solution. Then, the wet PU scaffold was put on a hot plate to dry the AgNWs solution. In order to turn the composite of AgNWs@PU scaffold to being active to achieve the pressure-sensitive characteristic, the loading force of >10 N was applied on it lasting for about 5 s. In Fig. 1b, the typical scanning electron microscopy (SEM) image showed the three-dimensional (3D) microporous morphology of the active composite of AgNWs@PU scaffold after several times of the soak-coating and drying processes and heavy loading. The active composite of AgNWs@PU scaffold consisted of interlaced and fractured PU bones, which were coated with the large length-diameter ratio of AgNWs (Fig. 1c and Fig. S2) that would make the PU bones be conductive. It should be noted that the resistance of the active composite of AgNWs@PU scaffold was influenced by the times of the soak-coating and drying process. Although the pure PU scaffold was a nonconductor, it would character the resistance of ~10 MΩ after first being coated with AgNWs (Fig. S1). In the wake of increasing the times of the soak-coating and drying processing, the resistance dramatically decreased. After 4 processing times, it would tend to be relatively stable and was around 3.5 kΩ, indicating that all the bones of the PU scaffold were coated with AgNWs. To fabricate the HeCM tactile sensor, two pieces of carbon fabric were respectively placed on the top and bottom of the active

composite of AgNWs@PU scaffold for sandwiching assembly, following by covering a 3M adhesive tape for encapsulation. The SEM image of the carbon fabric showed that the carbon fibers (Fig. S3) were uniform to form a cluster, and then the clusters were woven together to form a cross and undulant pattern (Fig. 1d). In the following experiments, it could be found that the undulant patterned characteristic of the carbon fabric provided microstructure engineering for designing tactile sensors. More detailed information about fabrication processes of the HeCM tactile sensor was described in the part of Experimental Section.

In this study, two types of HoCM tactile sensors were also prepared for comparison (**Fig. 2**a). The tactile sensor based on layered microstructure (LM tactile sensor) was made of two pieces of the carbon fabric, which were face-to-face assembled together. In the second case, the active composite of AgNWs@PU scaffold was directly employed to fabricate the tactile sensor based on porous microstructure (PM tactile sensor). As a contrast, the as-prepared LM tactile sensor, PM tactile sensor, and HeCM tactile sensor were all prepared in the size of 1 × 1 cm^2 unless otherwise stated.

To investigate the mechanosensational properties, variations in the resistance of the LM tactile sensor, PM tactile sensor, and HeCM tactile sensor under different force were tested. As shown in Fig. 2b, the resistance was recorded with the increase of external applied force. The onset values of resistance, which were the initial ones of the devices when no external force was applied, were around 250 Ω, 3.5 kΩ, and 5.9 kΩ corresponding to the LM tactile sensor, PM tactile sensor, and HeCM tactile sensor, respectively. The relatively larger initial resistance of the HeCM tactile sensor was attributed to the weak contact between the active composite of AgNWs@PU scaffold and the carbon fabric. The relation curves of resistance and pressure showed the resistances of all the tactile sensors significantly decrease with the increased external force, manifesting that the as-prepared tactile sensors could respond to the change of the external force. Applied by the same external force, the LM tactile sensor showed the lower value of resistance compared to the two others. This was since the carbon fibers that composed carbon fabric were uniform, which was

conducive to the movement of electrons. The above results showed the active composite of AgNWs@PU scaffold was porous, which made the difficulty of electrons movement and curved the conductive paths that would increase resistance. Therefore, these two aspects brought out the relatively lower resistance of the LM tactile sensor than that of other tactile sensors. Specifically, the resistance of the LM tactile sensor tended to be stable when the applied external force exceeded 0.5 N, which meant that the force detection by the LM tactile sensor was limited below 0.5 N. In the case of the PM tactile sensor, larger force detection range of 3 N was achieved. Electric contact theory pointed out that the area increase of electric contact would decrease the contact resistance. The different force detection ranges of these two tactile sensors were mainly caused by the different electric contact types that were layered electric contact and multipoint electric contact corresponding to the LM tactile sensor and PM tactile sensor, respectively. As the active composite of AgNWs@PU scaffold consisted of numerous conductive bones, contact points of these conductive bones were generated slowly with the external force. Until the masses of contact points reached saturation, the resistance of the PM tactile sensor would not be varied. This was unlike the contact case of the LM tactile sensor, which adopted carbon fabric that featured the undulant surface microstructure as the active sensing materials. There was not enough contact area of the upper and bottom carbon fabric to be changed since their limited separation distance. Thus, after applying a relatively small force, the resistance of the LM tactile sensor would not be dramatically changed even if increasing the external force. Through the HeCM design, the force detection range was remarkably extended by 116% compared to the one of the PM tactile sensor, and reached up to 6.5 N, which was 13 times larger than that of the LM tactile sensor. This was because the electric contact type of the HeCM tactile sensor included not only the electric contact among the conductive bones of the active composite of AgNWs@PU scaffold but also the multipoint electric contact between the active composite of AgNWs@PU scaffold and carbon fabric, leading to hierarchically and synergistically retarding saturation of each contact point to withstand larger external force. Multiple testing results indicated that by means of the

HeCM design, the range of force detection could be significantly enhanced compared to the one of the counterpart based on the HoCM (Fig. S4). The larger mechanosensational sensing range would bring tactile sensor into more wonderful applications in the future, especially for robotic control, manipulation of prosthetic limbs, and human-related interactive system. The design thought of this HeCM proposed here was universal and may be extended to further develop tactile sensors based on other sensing mechanisms involving magnetoresistive sensing, electromagnetic sensing, and capacitive sensing.

To evaluate the pressure-sensing properties, the relationships of the normalized current change and the pressure regarding the LM tactile sensor, PM tactile sensor, and HeCM tactile sensor were tested by applying the fixed voltage of 5 V (Fig. 2c). In the case of the LM tactile sensor, the variation in the normalized current could not be distinguished when the applied pressure exceeded 5 kPa was being applied, indicating that the LM tactile sensor could only be used to detect the pressure of <5 kPa. From the result in Fig. 2b, it could be found that the resistance of the LM tactile sensor dropped quickly as the increase of the external force and then remained when the external force was larger than 0.5 N. Therefore, according to Ohm law, the current through the LM tactile sensor would not change even by increasing the external force of > 5 kPa. Similarly, as the resistance of the PM tactile sensor would not be varied when the external force was larger than 3 N (Fig. 2b), the current tended to be stationary after the pressure was applied up to 30 kPa. In the case of the HeCM tactile sensor, as the device's resistance was continually changed until the external force reached up to 6.5 N (Fig. 2b), continuous variation in the normalized current was achieved even if the larger pressure of >30 kPa was applied, and until the pressure increased up to 65 kPa. Here, the sensitivity of the tactile sensor was defined as the slope of the curve $\Delta I/I_0/\Delta P$, where ΔI was the change in current, I_0 was the current through the tactile sensor without applied pressure, and ΔP denoted the change in applied pressure. An approximately linear relationship of the normalized current change and the pressure led to the ultrahigh sensitivity of 10.1 kPa^{-1} of the LM tactile sensor for the pressure below 5 kPa (Fig. S5a). For the PM tactile sensor, the

sensitivity was 2.6 kPa^{-1} in the range of 0-30 kPa (Fig. S5b). In contrast, the relationship of the normalized current change and the pressure regarding the HeCM tactile sensor was nonlinear, turning out that its sensitivities were 4.1 kPa^{-1} for the range of 0-10 kPa and 1.2 kPa^{-1} for the range from 10 to 65 kPa (Fig. S5c). Comparing with the recently developed tactile sensors (Fig. S6 and Table S1), the as-designed HeCM tactile sensor featured not only high sensitivity but also wide pressure sensing range, which would contribute to reducing the difficulty of back-end circuit design for further identifying, coding and use of the mechanotransduction electrical signals as following demonstrated.

In the following experiments, the HeCM tactile sensor was chosen as the testing model except as otherwise noted. The multiple loading-unloading tests of the HeCM tactile sensor under the pressure loading conditions of 5, 30, and 60 kPa were conducted (Fig. 2d). In the case of 5 kPa loading, the current signal through the HeCM tactile sensor rose to respond to the pressure. Larger and stable electrical signal change in the normalized current was observed when the loading pressure of 30 kPa was applied on the HeCM tactile sensor. Furthermore, the electrical signal was identified for increasing the loading pressure up to 60 kPa. The multiple tests clearly manifested that the changes in the normalized current made a distinction to respond to different pressure, and thus could be used to stably identify the wide range of pressure between 5 and 60 kPa. The current change under dynamic pressure condition at different loading frequencies of 0.5, 1, and 4 Hz with the pressure of 20 kPa were presented in Fig. 2e. Although a slight difference existed in the slopes of the peaks in each graph, which was caused by the adjustment of the loading parameters and the instability of the workbench during the loading process, it could be found that each period of the current change was almost matched with the pressure loading frequency. Thus, the HeCM tactile sensor featured fast pressure detectability and would satisfy most of the requirements for routine human-related interactive application. The results demonstrated that the hetero-contact microstructure could be used to design high-performance tactile sensor that characterized wide sensing range, high sensitivity, stable signal response, and fast detectability. The manufacturing strategy presented in

this work was feasible and effective. We believe that the hetero-contact microstructure proposed here is universal and may be extended to further develop tactile sensors based on other sensing mechanisms involving magnetoresistive sensing, electromagnetic sensing and capacitive sensing, and the pressure-sensing paradigm would provide a novel design-concept to advance light, sound, temperature, and humidity sensing devices.

To better understand the working mechanism, the sensing schematic diagrams of the LM tactile sensor, PM tactile sensor, and HeCM tactile sensor were illustrated in **Fig. 3**. Based on the assembly design of the LM tactile sensor, the initial upper and bottom conductive layers, which are composited of two pieces of carbon fabric, contact in a small area in the situation of unloading external pressure resulting in a relatively large resistance (Fig. 3a-I). As a gentle press is applied, the contact area of upper and bottom carbon fiber clusters (Fig. S7a) is sharply increased, and then approaches saturation since there is no enough carbon fiber cluster to be contacted between the upper and bottom conductive layers (Fig. 3a-II). During the process of applying pressure, the resistance of the LM tactile sensor dramatically drops with the increase of pressure. Therefore, the total resistance (R_t) can be expressed as: $R_t = R_{ff1} + R_{ff2} + R_{ff3} + ...$, where R_{ff1}, R_{ff2} and R_{ff3} are the changeable contact resistance of different contact area of the carbon fiber clusters between the upper and bottom carbon fabric (Fig. S7b). In the case of the PM tactile sensor, the active composite of AgNWs@PU scaffold, which is the main sensing subject of the device, is porous leading to the difficulty of electrons movement and curving the conductive paths (Fig. 3b-I). As a result, the PM tactile sensor exhibits high resistance in the relaxation state. When an external pressure is applied on the PM tactile sensor, the conductive bones of the active composite of AgNWs@PU scaffold will be deformed, and thus contact in a small part (Fig. 3b-II and Fig. S7c). Based on electric contact theory, the contact resistance will continue to decrease until no other contact point was generated [43]. In this case, the active composite of AgNWs@PU scaffold possesses masses of fractured and free conductive bones that will be contacted with each other. It is unlike the case of the LM tactile sensor that the contact area is finished in one step. As the contact

points of the conductive bones increased slowly to respond to the external pressure, contact saturation needs relatively larger external pressure to be applied on the active composite of AgNWs@PU scaffold. Consequently, the resistance of the PM tactile sensor will continue to change until there is no free conductive bone to participate in interlaced contact, bringing out larger pressure detection range of the PM tactile sensor than that of the LM tactile sensor. On the other hand, the contact area of conductive bones is obviously smaller than that of carbon fiber clusters, giving rise to further slowness of the change in the resistance of the active composite of AgNWs@PU scaffold. Therefore, the PM tactile sensor features relatively low sensitivity compared to the LM tactile sensor in the low-pressure range. As a whole, the active composite of AgNWs@PU scaffold is like a variable resistor that can sense the change of the external pressure according to the corresponding value of resistance. Thus, as shown in Fig. S7d, the total resistance of the PM tactile sensor (R_t') is simplified as: $R_t' = R_{bb1} + R_{bb2} + R_{bb3} + ...$, where R_{bb1}, R_{bb2} and R_{bb3} are the changeable contact resistance of different contact points of the conductive bones of the active composite of AgNWs@PU scaffold.

Inside the mammalian skin, Meissner corpuscle, Pacinian corpuscle, Merkel cell, and Ruffini corpuscle are four tactile mechanoreceptors with different adapting types that synergistically perceive external mechanical stimuli. Inspired by this synergistically sensory mechanism of different types of tactile mechanoreceptors, herein we propose the hetero-contact microstructure to strategically design tactile sensor in order to significantly enhance sensing range. For the case of the HeCM tactile sensor, the contact area includes not only the multipoint electric contact among the conductive bones of the active composite of AgNWs@PU scaffold but also the other multipoint electric contact between the conductive bones and the carbon fiber clusters (Fig. 3c-I and Fig. S7e). When small external pressure is applied on the HeCM tactile sensor, these two types of the multipoint electric contact are both involved. At this stage, the resistance drops rapidly as a large number of contact points begin to appear, especially the contact points between the conductive bones and the carbon fiber clusters (Fig. 3c-II). Here, the involvement of carbon fiber cluster

features relatively small resistance that will bring out rapid change in device's resistance. Consequently, high sensitivity will be obtained for the HeCM tactile sensor within a certain range of pressure. It should be noted that the device's electric contact is contributed to not only the electric contact of the conductive bones of the active composite of AgNWs@PU scaffold but also the electric contact between the conductive bones and the carbon fiber clusters. Once potential contact points are all accomplished and cannot be tighter, the resistance of the HeCM tactile sensor will be stable no matter the external pressure further increases. Therefore, the designed hetero-contact microstructure of the tactile sensor leads to hierarchically and synergistically retarding saturation of each contact point to withstand the external pressure, so that wide range of pressure detection can be realized. The total resistance of the HeCM tactile sensor (R_t'') is thus simplified as: $R_t'' = (R_{bb1} + R_{bb2} + R_{bb3} + ...) + (R_{cb1} + R_{cb2} + R_{cb3} + R_{cb4} + R_{cb5} + R_{cb6} + ...)$, where R_{cb1}, R_{cb2}, R_{cb3}, R_{cb4}, R_{cb5} and R_{cb6} are the changeable contact resistance of different contact points between the carbon fiber clusters of the carbon fabric and the conductive bones of the active composite of AgNWs@PU scaffold (Fig. S7f). As a summary, although the pressure sensing range of the tactile sensor based on the simple HoCM including layered microstructure and porous microstructure demonstrated here is limited and small, it will be strategically and significantly enhanced by adopting the programmed HeCM that synergistically perceives external mechanical pressure through the assembly of multipoint electric contact, which coincides with the experimental results presented in Fig. 2.

Force feedback plays a critical role for control of prosthetic limbs and manipulator fine motions of teleoperation since the force strength of control is generally loose and often not just as desired. In the following study, we constructed a visual force feedback system, which made the possibility to turn thought into desired action that the force strength would be reflected and observed by a virtual color (**Fig. 4**a). When a tester's finger pressed on a table, the electrical signal from the HeCM tactile sensor that was attached on the glove's fingertip quickly rose, and then was coded as the dynamically alterable color to make a force feedback (Fig. 4b). Correspondingly, the visible color would be changed from violet to red with intermediately graded levels to

give the visual force feedback that represented the tactile information of no touch and different force strength. As the force strength between the table and the tester's fingertip began to be released, the electrical signal from the HeCM tactile sensor decreased accordingly. The dynamically alterable color quickly made an associated response that could be observed by the tester to assess the force strength and then adjust it to a desired level. Two successive press-release cycles of the visual force feedback were presented in Video S1. As the force strength between the table and fingertip was implemented dynamically and non-linearly by the tester, the signal variation reflecting the force strength *versus* time was not linear during two successive press-release cycles in the demo. Notably, owing to the wide pressure sensing range, reproducible pressure response (Fig. S8a), durable pressure detectability (Fig. S8b), and fast response time (Fig. S8c and Fig. S8d), the HeCM tactile sensor possessed significant potential in force feedback for natural manipulations and grasping in robotics and artificial limbs.

Interactive entertainment experience is of significant interest to make our lives more fascinating. We exploited the practical capability of the HeCM tactile sensor as a human-computer interface towards entertainment interactive experience. A wearable three-dimensional (3D) tactile panel assembled with seven HeCM tactile sensors was presented in Fig. 4c. Assisting with a simple analog-to-digital conversion (ADC) circuit (Fig. S9), the wearable 3D tactile panel provided a novel communication channel that could turn a virtual thought into realistic sound. Noteworthily, due to the stable electromechanical response and large changing range of signal, the coding and use of the mechanotransduction signals from the HeCM tactile sensors did not need any denoise processing or signal amplification that significantly reduced the difficulty of circuit design for multiple units integrated system. As a proof-of-concept demonstration, the electrical signals from the seven HeCM tactile sensors were respectively coded and used to produce sounds according to the tonic solfa of "Do", "Re", "Mi", "Fa", "Sol", "La", "Si". In this work, we stratified the pressure into three parts that defined the pressure of <10 kPa, the pressure range between 10-50 kPa, and the pressure exceeding 50 kPa as gentle press, moderate press, and heavy press,

respectively. Correspondingly, soft voice, normal voice, and loud voice would be made by respectively applying the gentle press, moderate press, and heavy press on each HeCM tactile sensor. In addition, computer screen would also display different gray levels to reflect the three ranges of pressure, where the lightest color and deepest color corresponded to the gentle press and heavy press, respectively (Fig. S10). For example, when a gentle press was applied by a fingertip gently touching on the first HeCM tactile sensor, soft voice in the tone of "Do" would be sent out from the computer (Fig. 4d). As the other example of the realistic sound feedback, the normal voice in the tone of "Re" would be made when a moderate press was imported through the second HeCM tactile sensor. Furthermore, once a heavy press was applied on the third HeCM tactile sensor, the change in electrical signal quickly arose. Thereafter a corresponding instruction would be sent to the computer to make loud voice in the tone of "Mi". Other different sound intensity in the tonic solfa of "Fa", "Sol", "La", "Si" would also be obtained by applying the corresponding pressure strength on the appointed HeCM tactile sensor. It should be noted that the electrical signals of the HeCM tactile sensors were stable even if the working environment is noisy (Video S2). We believe that versatile interactive entertainment experience would spring out by exploiting the HeCM tactile sensors to make life more interesting.

Virtual reality (VR) that creates unique and interactive environments is increasingly being employed to turn thought into visual actions that would facilitate studies of natural events, surgical operation, rehabilitation therapy, and prosthetics for modelling, experiencing, and training. To a certain extent, manipulation is difficult in VR system especially for immersive virtual environment due to the fact that people don't easily find a specified button for desired interaction. As a proof-of-concept, by assembling a glove with five HeCM tactile sensors, a force feedback data glove that could sense fingertip pressure was fabricated for free control of virtual navigation (**Fig. 5**a). Before experiencing in an immersive virtual environment, a wireless typing was carried out by controlling cursor position through the data glove for training (Fig. 5b). A multichannel microprogrammed control unit (MCU) was utilized to identify and

then code the change in electrical signals from the five HeCM tactile sensors, which were attached on each fingertip of the data glove (Fig. S11). After a series of signal processing involving ADC, normalized values, compared with a threshold, the pressure from each fingertip would be translated into specified instruction that could be sent to the virtual typing environment through Bluetooth communication technology. In the virtual wireless typing system, the shifting instructions of "Move up", "Move down", "Move left", "Move right", and "Input" were respectively controlled by index finger, middle finger, ring finger, little finger, and thumb. The changes in electrical signals from the five HeCM tactile sensors could be detected individually and precisely so that the pressure from each fingertip would be identified (Fig. 5c). As a further detail, the letters from "A" to "Z" and the functional keys of "Tab", ".", "Space", "," and "Enter" were divided and presented in a certain position of a virtual keyboard. The cursor position would be shifted to adjoining position when the virtual keyboard received the functional instructions of "Move up", "Move down", "Move left", or "Move right" after index finger, middle finger, ring finger, or little finger pressing on a subject, such as a table. Once the MCU detected the change in electrical signal from the HeCM tactile sensor attached on the thumb tip, a selected letter or functional key would be input into the above text box. To verify it, text of "HELLO NTU", as an example, was successfully typed into the text box by pressing on the table through the data glove (Video S3). Therefore, the wireless typing using the data glove assembled with the HeCM tactile sensors was feasible and would be realized in the future studies to work in the VR system involving virtual and creative design of scene-based advertisement text.

A virtual jungle environment was created for the immersive virtual interaction. The data glove assembled with the five HeCM tactile sensors was served as the wireless human-computer interface for immersive whole-body navigation in the virtual jungle environment. Inside a VR headset, we encode the navigational instructions of "Go ahead", "Step back", "Move left", "Move right", and "Jump up" to the pressure signals from index finger, middle finger, ring finger, little finger, and thumb of the data glove, respectively. It should be noted that the virtual scene would not be

changed when the hand shook since no signal would be output from the data glove to the VR headset (Fig. 5d). Only when the tester's hand wearing the data glove touched a subject, the precise and free control of the virtual navigation would be carried out (Fig. 5e and 5f). To make the difference clearly, variation of the electrical signal from the five HeCM tactile sensors in different hand touching situations were tested (Fig. 5g). When the hand shook, the changes in electrical signals were negligible as there was no external pressure applied on the HeCM tactile sensors. The five HeCM tactile sensors exhibited fast and robust responses to manual pressure between the fingers and an arm or between the fingers and a table. For a detailed example, the change in electrical signal of the HeCM tactile sensor attached on the index finger would be generated when the finger touched a subject, such as an arm or a table. Assisted with the signal processing circuit and wireless communication technology, the navigational instruction of "Go ahead" would be sent to the VR headset and finally give a visible feedback to make the tester feel himself moving forward in the virtual jungle environment. Through the press from different fingers and visual feedback of the virtual scene, we could readily turn our thought into the motions in the virtual jungle environment to easily and freely experience immersive human-computer interaction (Video S4). These initial results make it confident that the HeCM tactile sensor is a conceptually viable platform for contributing to more scene control, deft manipulation of objects, and even demo simulation of surgical operation in the future.

Furthermore, a planar integration of the HeCM tactile sensor array was successfully constructed to spatially map pressure information. The HeCM tactile sensor array with 4 × 4 pixels was schematically describes in **Fig. 6**a. The "cutting-and-assembling" method was used to fabricate the sensor array that each HeCM tactile sensor was sandwiched and assembled at the cross of row electrodes and column electrodes (Fig. S12). The as-constructed sensor array was endowed with 3D mapping sensing capability that could identify multipoint pressures by cross-scanning signals from the row electrodes and column electrodes (Fig. 6b). As the HeCM tactile sensor featured high sensitivity, wide sensing range and high stability, the different pressure of gentle press, moderate press and heavy press was readily distinguished and reflected as light

green pattern, blue pattern and red pattern, respectively (Fig. 6c). In addition, motion trajectory could also be monitored by using the HeCM tactile sensor array. As a proof-of-concept demonstration, when a fingertip pressed on the HeCM tactile sensor array along the path from p11, p12, p13 to p14 (Fig. 6d), from p11, p21, p31 to p41 (Fig. 6e), or from p11, p22, p33 to p44 (Fig. 6f), the fingertip's motion trajectory could be clearly tracked in cross-locating (Fig. 6g-i). Notably, each HeCM tactile sensor could identify the pressure information along the motion trajectory that was further reflected by different color when the fingertip pressed on it. We believed that the monitoring and identification capability would give the HeCM tactile sensor array the potential to drive the development of personalized safety identification in the future.

4. Conclusions

In summary, inspired by the synergistically sensory mechanism of different types of tactile mechanoreceptors, we proposed the hetero-contact microstructure (HeCM) to fabricate tactile sensor that adopted the active composite of AgNWs@PU scaffold combined with carbon fabric. By adopting the programmed HeCM that synergistically perceives external mechanical pressure, the force detection range was strategically and remarkably extended by 116% and reached up to 6.5 N, which was 13 times larger than that of the common tactile sensor. High sensitivities, fast response, and high stability of the HeCM tactile sensor were also achieved, and thus significantly reduced the processing difficulty of the coding and use of the mechanotransduction signals. Visual force feedback system, wearable three-dimensional tactile panel, and force feedback data glove were constructed and demonstrated the significant potential of the HeCM tactile sensor for force-feedback-enhanced grasping in robotics and artificial limbs, entertainment interactive experience, and virtual reality interaction that made the possibility to precisely and freely turn thought into desired control.

Acknowledgements

The research was supported by the National Research Foundation of Singapore (No. NRF-CRP11-2012-01), the National Key Research and Development Program of

China (No. 2017YFB1002504), and the National Natural Science Foundation of China (No. 61631010 and 51872048).

Appendix A. Supporting information

References

[1] X. Wang, L. Dong, H. Zhang, R. Yu, C. Pan, Z.L. Wang, Adv. Sci., 2 (2015) 1500169.

[2] L. Wang, D. Chen, K. Jiang, G. Shen, Chem. Soc. Rev., 46 (2017) 6764-6815.

[3] A. Chortos, J. Liu, Z. Bao, Nat. Mater., 15 (2016) 937-950.

[4] Z.L. Wang, Mater. Today, 20 (2017) 74-82.

[5] D. Rus, M.T. Tolley, Nature, 521 (2015) 467-475.

[6] X.J. Pu, H.Y. Guo, J. Chen, X. Wang, Y. Xi, C.G. Hu, Z.L. Wang, Sci. Adv., 3 (2017) e1700694.

[7] X. Cao, M. Zhang, J. Huang, T. Jiang, J. Zou, N. Wang, Z.L. Wang, Adv. Mater., 30 (2018) 1704077.

[8] C. Wang, J. Zhao, C. Ma, J. Sun, L. Tian, X. Li, F. Li, X. Han, C. Liu, C. Shen, L. Dong, J. Yang, C. Pan, Nano Energy, 34 (2017) 578-585.

[9] L.E. Osborn, A. Dragomir, J.L. Betthauser, C.L. Hunt, H.H. Nguyen, R.R. Kaliki, N.V. Thakor, Sci. Robot., 3 (2018) eaat3818.

[10] X. Liao, Q. Liao, Z. Zhang, X. Yan, Q. Liang, Q. Wang, M. Li, Y. Zhang, Adv. Funct. Mater., 26 (2016) 3074-3081.

[11] X. Liao, Q. Liao, X. Yan, Q. Liang, H. Si, M. Li, H. Wu, S. Cao, Y. Zhang, Adv. Funct. Mater., 25 (2015) 2395-2401.

[12] K. Kim, M. Jung, B. Kim, J. Kim, K. Shin, O.-S. Kwon, S. Jeon, Nano Energy, 41 (2017) 301-307.

[13] F. Yi, X. Wang, S. Niu, S. Li, Y. Yin, K. Dai, G. Zhang, L. Lin, Z. Wen, H. Guo, J. Wang, M.H. Yeh, Y. Zi, Q. Liao, Z. You, Y. Zhang, Z.L. Wang, Sci. Adv., 2 (2016) e1501624.

[14] Y. Han, F. Yi, C. Jiang, K. Dai, Y. Xu, X. Wang, Z. You, Nano Energy, 56 (2019)

516-523.

[15] F. Yi, J. Wang, X. Wang, S. Niu, S. Li, Q. Liao, Y. Xu, Z. You, Y. Zhang, Z.L. Wang, ACS Nano, 10 (2016) 6519-6525.

[16] Q. Hua, J. Sun, H. Liu, R. Bao, R. Yu, J. Zhai, C. Pan, Z.L. Wang, Nat. Commun., 9 (2018) 244.

[17] X. Pu, H. Guo, Q. Tang, J. Chen, L. Feng, G. Liu, X. Wang, Y. Xi, C. Hu, Z.L. Wang, Nano Energy, 54 (2018) 453-460.

[18] T. Li, Y. Xu, M. Willander, F. Xing, X. Cao, N. Wang, Z.L. Wang, Adv. Funct. Mater., 26 (2016) 4370-4376.

[19] X. Liao, X. Yan, P. Lin, S. Lu, Y. Tian, Y. Zhang, ACS Appl. Mater. Interfaces, 7 (2015) 1602-1607.

[20] M. Ma, Z. Zhang, Q. Liao, F. Yi, L. Han, G. Zhang, S. Liu, X. Liao, Y. Zhang, Nano Energy, 32 (2017) 389-396.

[21] S. Wang, J. Xu, W. Wang, G.N. Wang, R. Rastak, F. Molina-Lopez, J.W. Chung, S. Niu, V.R. Feig, J. Lopez, T. Lei, S.K. Kwon, Y. Kim, A.M. Foudeh, A. Ehrlich, A. Gasperini, Y. Yun, B. Murmann, J.B. Tok, Z. Bao, Nature, 555 (2018) 83-88.

[22] Z. Lou, S. Chen, L. Wang, K. Jiang, G. Shen, Nano Energy, 23 (2016) 7-14.

[23] H. Cheng, Y. Huang, L. Qu, Q. Cheng, G. Shi, L. Jiang, Nano Energy, 45 (2018) 37-43.

[24] M.-J. Yin, Z. Yin, Y. Zhang, Q. Zheng, A.P. Zhang, Nano Energy, 58 (2019) 96-104.

[25] F. Yi, L. Lin, S. Niu, P.K. Yang, Z. Wang, J. Chen, Y. Zhou, Y. Zi, J. Wang, Q. Liao, Y. Zhang, Z.L. Wang, Adv. Funct. Mater., 25 (2015) 3688-3696.

[26] X. Liao, W. Wang, L. Wang, K. Tang, Y. Zheng, ACS Appl. Mater. Interfaces, 11 (2019) 2431-2440.

[27] X. Liao, Z. Zhang, Q. Liang, Q. Liao, Y. Zhang, ACS Appl. Mater. Interfaces, 9 (2017) 4151-4158.

[28] Y. Zhang, Y. Yang, Y. Gu, X. Yan, Q. Liao, P. Li, Z. Zhang, Z. Wang, Nano Energy, 14 (2015) 30-48.

[29] W. Wu, Z.L. Wang, Nat. Rev. Mater., 1 (2016) 16031.

[30] X. Wang, H. Zhang, L. Dong, X. Han, W. Du, J. Zhai, C. Pan, Z.L. Wang, Adv. Mater., 28 (2016) 2896-2903.

[31] X.Y. Wei, X. Wang, S.Y. Kuang, L. Su, H.Y. Li, Y. Wang, C. Pan, Z.L. Wang, G. Zhu, Adv. Mater., 28 (2016) 6656-6664.

[32] C.C. Kim, H.H. Lee, K.H. Oh, J.Y. Sun, Science, 353 (2016) 682-687.

[33] M.S. Sarwar, Y. Dobashi, C. Preston, J.K. Wyss, S. Mirabbasi, J.D. Madden, Sci. Adv., 3 (2017) e1602200.

[34] L. Pan, A. Chortos, G. Yu, Y. Wang, S. Isaacson, R. Allen, Y. Shi, R. Dauskardt, Z. Bao, Nat. Commun., 5 (2014) 3002.

[35] Y. Si, X. Wang, C. Yan, L. Yang, J. Yu, B. Ding, Adv. Mater., 28 (2016) 9512-9518.

[36] L. Sheng, Y. Liang, L. Jiang, Q. Wang, T. Wei, L. Qu, Z. Fan, Adv. Funct. Mater., 25 (2015) 6545-6551.

[37] H. Zhuo, Y. Hu, X. Tong, Z. Chen, L. Zhong, H. Lai, L. Liu, S. Jing, Q. Liu, C. Liu, X. Peng, R. Sun, Adv. Mater., 30 (2018) e1706705.

[38] G.Y. Bae, S.W. Pak, D. Kim, G. Lee, H. Kim do, Y. Chung, K. Cho, Adv. Mater., 28 (2016) 5300-5306.

[39] C. Pang, G.Y. Lee, T.I. Kim, S.M. Kim, H.N. Kim, S.H. Ahn, K.Y. Suh, Nat. Mater., 11 (2012) 795-801.

[40] J. Park, Y. Lee, J. Hong, M. Ha, Y.D. Jung, H. Lim, S.Y. Kim, H. Ko, ACS Nano, 8 (2014) 4689-4697.

[41] M. Jian, K. Xia, Q. Wang, Z. Yin, H. Wang, C. Wang, H. Xie, M. Zhang, Y. Zhang, Adv. Funct. Mater., 27 (2017) 1606066.

[42] X. Wang, Y. Gu, Z. Xiong, Z. Cui, T. Zhang, Adv. Mater., 26 (2014) 1336-1342.

[43] R. Holm, E.A. Holm, Electric contacts: theory and application, Springer-Verlag Berlin Heidelberg, New York, New York, 1967.

Figures

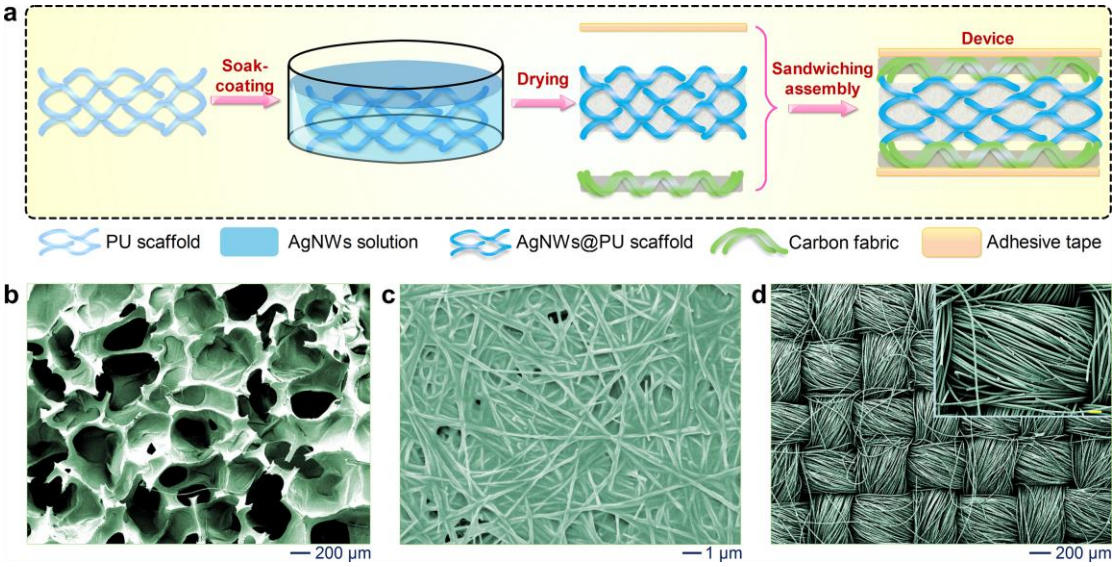

Fig. 1. Construction and characterization of tactile sensors. (a) Schematic illustration of the main processing steps of HeCM tactile sensor involving soak-coating, drying, and sandwiching assembly. (b) FESEM image of the polyurethane scaffold (PU scaffold) being coated with silver nanowires (AgNWs), showing the 3D microporous morphology of the active composite. (c) FESEM image of AgNWs, coating on the PU scaffold. The PU bones were conductive after be coated with the AgNWs. (d) FESEM image of carbon fabric. Inset was the enlarged image of the carbon fiber cluster, where the scale bar was 50 μm.

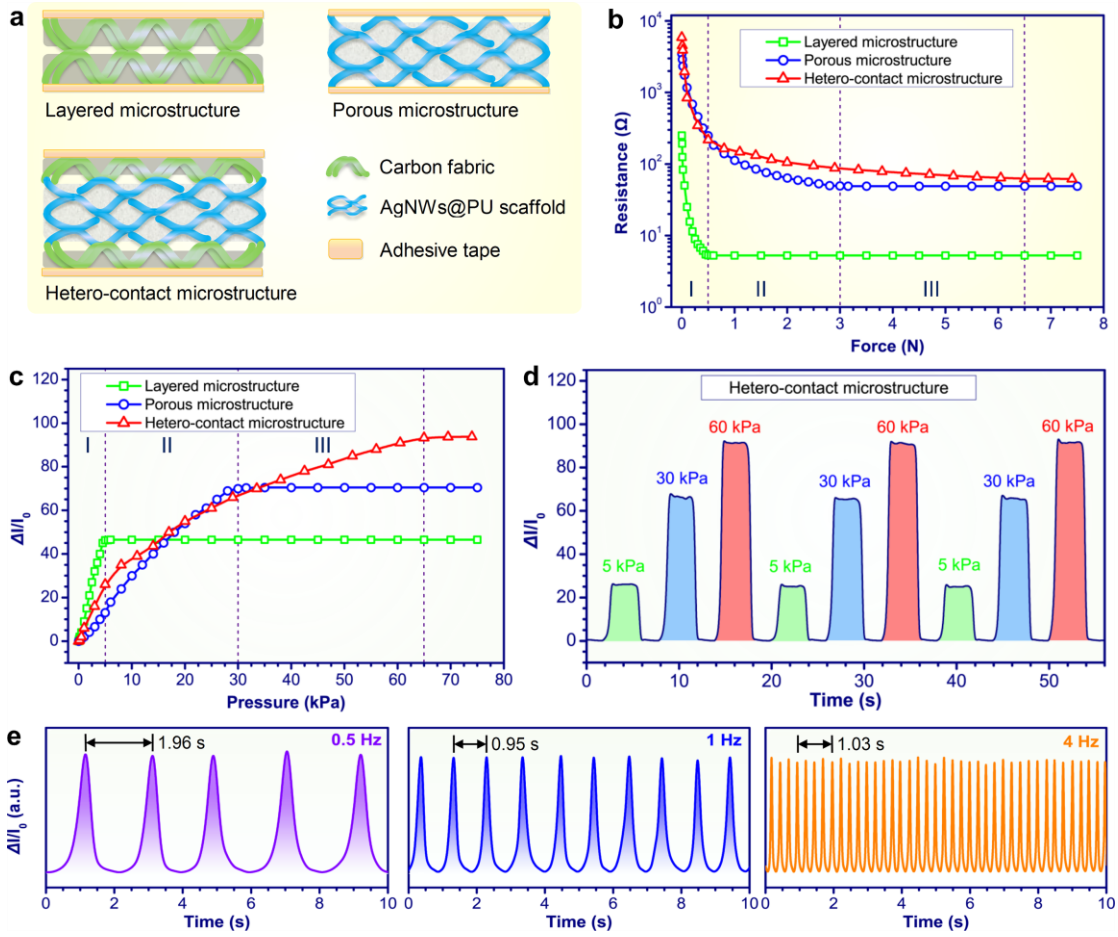

Fig. 2. Properties of tactile sensors. (a) Three types of structural diagram of the tactile sensors based on layered microstructure (LM), porous microstructure (PM), and hetero-contact microstructure (HeCM), respectively. (b) Typical resistance of the LM tactile sensor, PM tactile sensor, and HeCM tactile sensor *versus* force. (c) Variation in normalized current of the LM tactile sensor, PM tactile sensor, and HeCM tactile sensor under different pressure. (d) Current responses of the HeCM tactile sensors applied the pressure of 5, 30, and 60 kPa in the multiple loading-unloading processes. (e) Multiple-cycles tests of repeated loading-unloading pressure at the loading frequencies of 0.5, 1, and 4 Hz, where the time of one or four period of current change was pointed out.

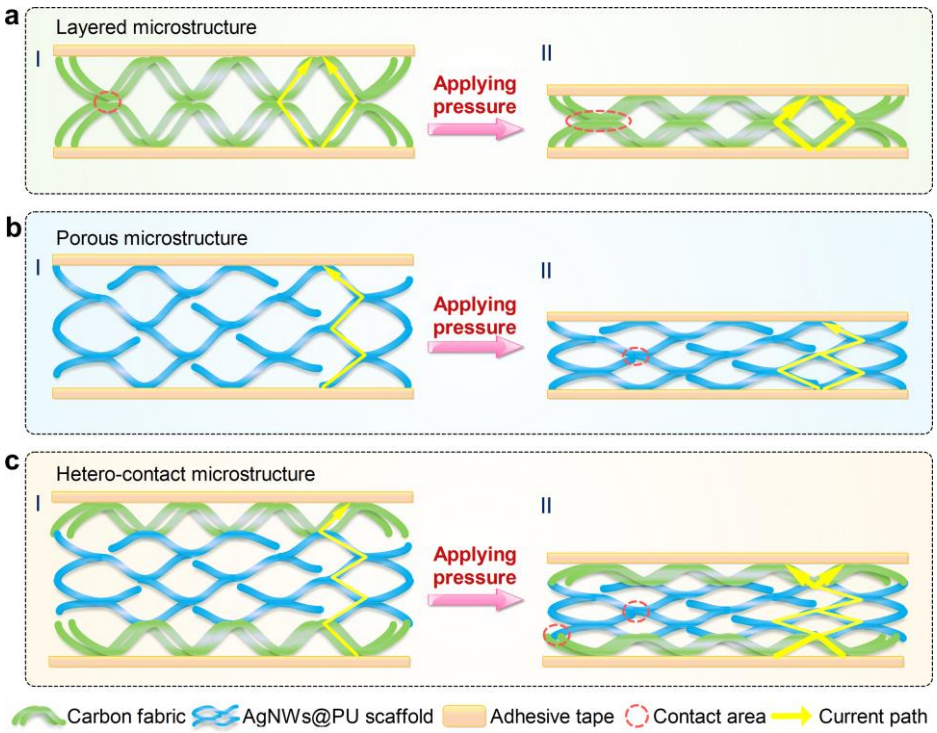

Fig. 3. Transduction mechanism of tactile sensors. (a) Schematic diagram of the LM tactile sensor (I) in the situation of unloading external pressure and (II) under applying pressure, where the contact area of upper and bottom carbon fiber clusters will be enlarged with the increase of the external pressure. (b) Schematic diagram of the PM tactile sensor (I) in the situation of unloading external pressure and (II) under applying pressure, where the conductive bones of the active composite of AgNWs@PU scaffold are deformed and thus contact with each other after applying pressure. (c) Schematic diagram of the HeCM tactile sensor (I) in the situation of unloading external pressure and (II) under applying pressure, where the contact area includes not only the multipoint electric contact among the conductive bones of the active composite of AgNWs@PU scaffold but also the other multipoint electric contact between the conductive bones and the carbon fiber clusters.

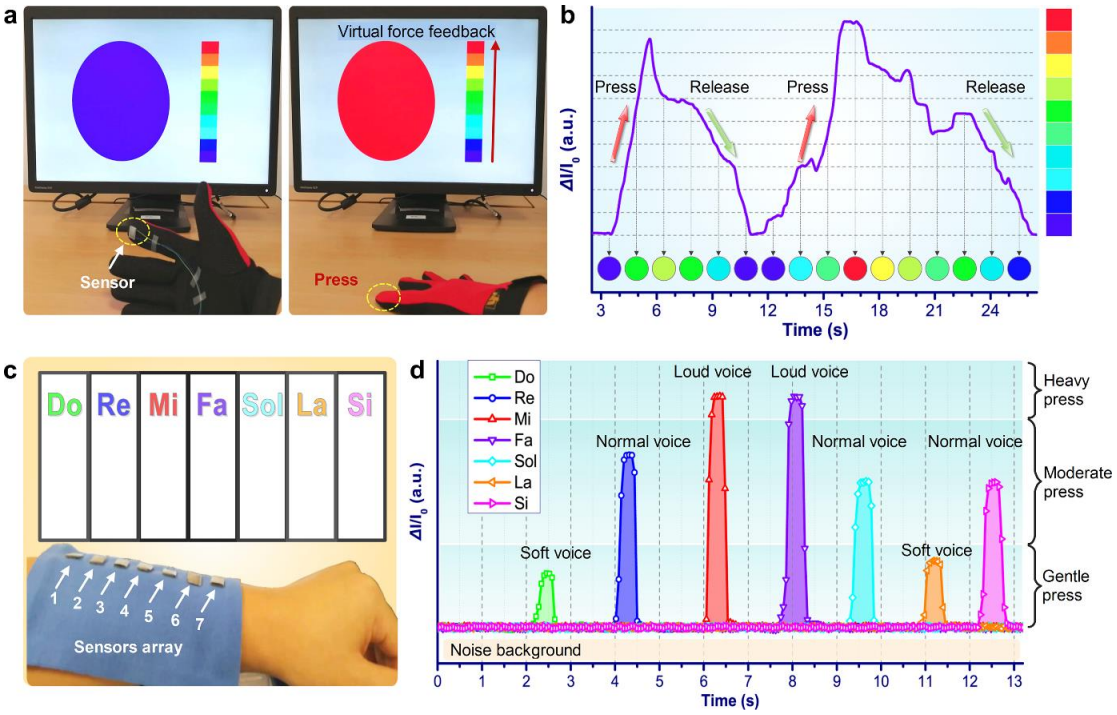

Fig. 4. Discerning fingertip interaction of tactile sensors. (a) Photographs of a visual force feedback system. The HeCM tactile sensor was attached on a glove's fingertip, which was pointed out by the circle of yellow dotted line. (b) Variation in the electrical signal from the HeCM tactile sensor during two successive press-release cycles. (c) Photograph of the wearable 3D tactile panel assembled with seven HeCM tactile sensors. The change in electrical signals from the seven HeCM tactile sensors were respectively coded and used to produce sounds according to the tonic solfa. (d) Variation in electrical signals of the seven HeCM tactile sensors, which was subjected to different pressure. Soft voice, normal voice, and loud voice would be made by respectively applying the gentle press (<10 kPa), moderate press (10-50 kPa), and heavy press (>50 kPa) on each HeCM tactile sensor.

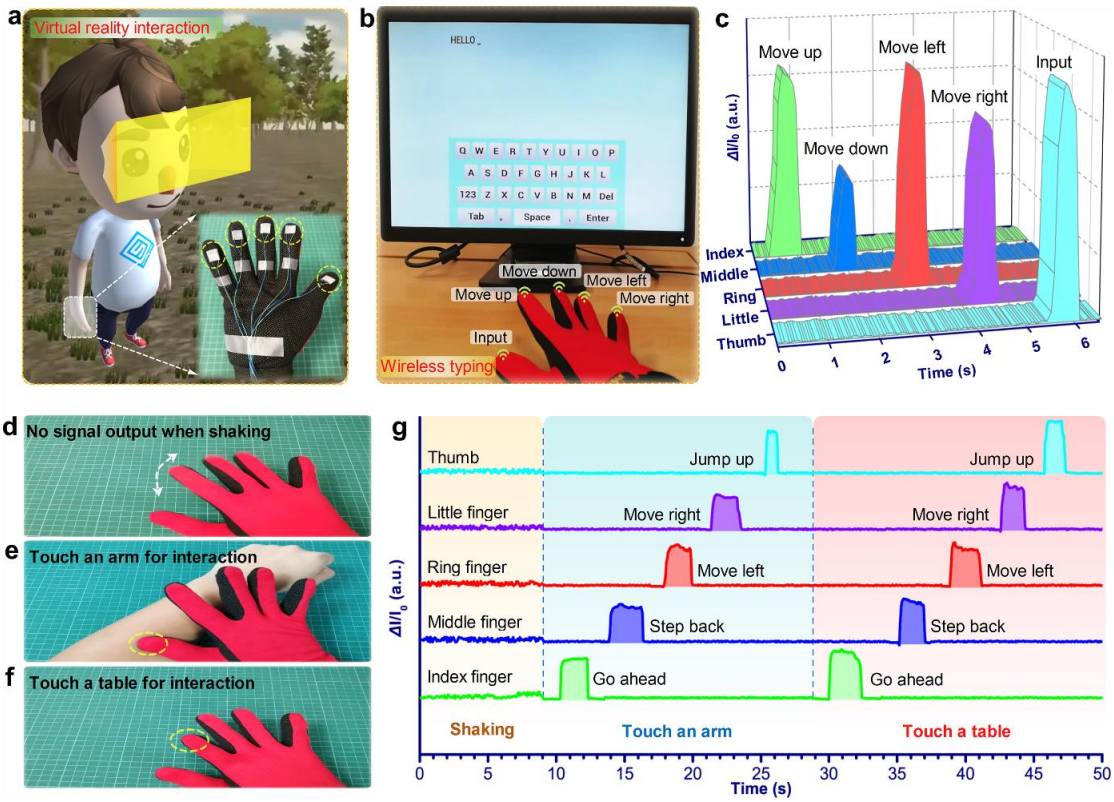

Fig. 5. Tactile sensors for virtual reality application. (a) Concept of the virtual relity interaction, where the configuration of the data glove was shown and the layout of the HeCM tactile sensors were pointed out by the circles of yellow dotted line. (b) Setup for evaluating input of virtual wireless typing system, where the shifting instructions were controlled by fingers. (c) Variation in the electrical signals from the five HeCM tactile sensors, which could be detected individually and precisely so that the pressure from each fingertip would be identified. (d) Photograph of shaking hand. The virtual jungle would not be changed since no signal would be output from the data glove to VR headset. (e, f) Photographs of touching an arm or a table for virtual interation, where the touching points were pointed out by the circles of yellow dotted line. (g) Variation in the electrical signals from the five HeCM tactile sensors in different hand touching situations, which were encoded as the navigational instructions.

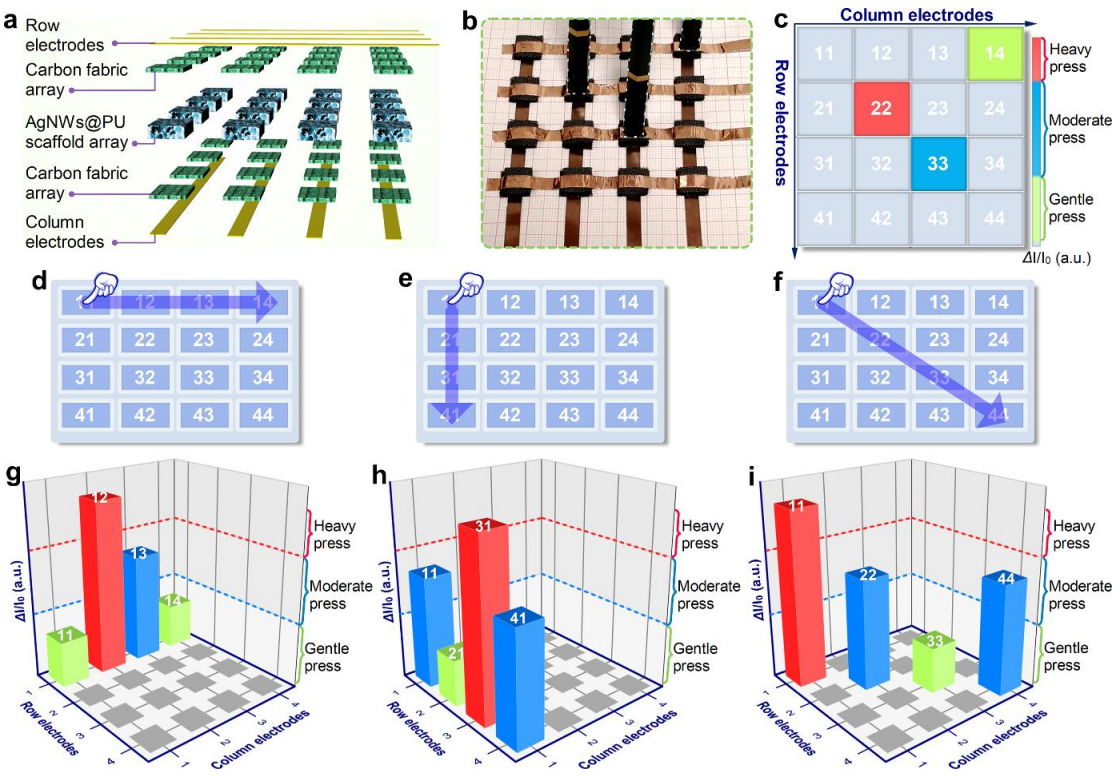

Fig. 6. Pressure mapping and motion trajectory tracking. (a) Schematic illustration of the planar integration of the HeCM tactile sensor array with 4 × 4 pixels. (b) Photograph of the device when three sensing points were pressed and (c) its corresponding mapping of the pressure distribution, where the different defined pressure of gentle press, moderate press and heavy press was reflected as light green pattern, blue pattern and red pattern, respectively. (d-f) Illustrations of the fingertip's motion trajectory along the path (d) from p11, p12, p13 to p14, (e) from p11, p21, p31 to p41, and (f) from p11, p22, p33 to p44. (g-i) Mapping record of the pressure distribution of the fingertip's motion trajectory.